ACS APPLIED MATERIALS & INTERFACES

Research Article

www.acsami.org

One-Pot Controlled Synthesis of Spongelike $CuInS_2$ Microspheres for Efficient Counter Electrode with Graphene Assistance in Dye-Sensitized Solar Cells

Mingyang Liu,[†] Guang Li,*[,†] and Xiaoshuang Chen*[,‡]

[†]School of Physics and Materials Science, Anhui University, Hefei, Anhui 230039, China

[‡]National Laboratory for Infrared Physics, Shanghai Institute of Technical Physics, Chinese Academy of Sciences, Shanghai 200083, China

Supporting Information

ABSTRACT: Spongelike $CuInS_2$ 3D microspheres were synthesized through a solvothermal method employing CuCl, $InCl_3$, and thiourea as Cu, In, and S sources, respectively, and PVP as surfactant. The as-prepared products have regular spherical shapes with diameters of 0.8−3.7 μm, the spheres consisted of small nanosheets, which are composed of small nanoparticles. As an important solar cell material, its photovoltaic property was also tested and the results showed a solar energy conversion efficiency of 3.31%. With the help of reduced graphene, its conversion efficiency could be further increased to 6.18%. Compared with conventional Pt material used in counter electrodes of solar cells, this new material has an advantages of low-cost, facile synthesis and high efficiency with graphene assistance.

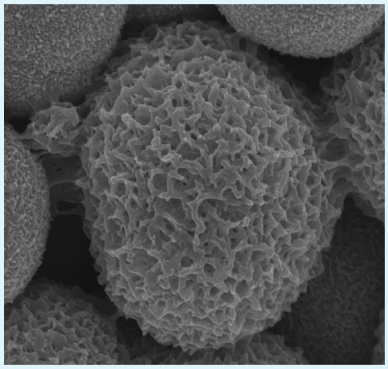

KEYWORDS: *$CuInS_2$, microspheres, photovoltaic property, graphene assisted, counter electrodes, power conversion efficiency*

INTRODUCTION

$CuInS_2$ is an important I−III−IV_2 ternary semiconductor material used as an absorber layer for high efficiency and radiation-hard solar cell applications due to its direct band gap of 1.5 eV and a large absorption coefficient ($\alpha \sim 105$ cm^{-1}).[1] Recent works on $CuInS_2$ nanocrystals (NCs) revealed that they have great potential as solar harvesters for a new generation of solution-processed solar cells,[2−6] and power conversion efficiencies of using $CuInS_2$ NCs in solar cell devices have approached ∼5%.[3−5] Besides NCs, other $CuInS_2$ nanostructures such as nanorods, nanotubes, nanoacorns, nanobottles, nanodisks, and larva-shape nanostructures have been reported using different synthetic routes.[7−11] Because of the strong correlation between the physical and chemical properties and the shape, size, and structure of nanomaterials, it is clear that the photoelectrochemical performance depends on the morphology of $CuInS_2$ nanostructure. Especially, curved three-dimensional (3D) microspheres consisting of primary nanoscale building units may exhibit promising applications. However, up to now, it is still a challenge to prepare $CuInS_2$ 3D microspheres.[12]

The availability of cost- and energy-efficient, scalable photovoltaic technologies will be a key to the future exploitation of solar energy. Because of the low cost, environmental friendliness, and simple preparation procedures, dye-sensitized solar cells (DSSCs) have been paid considerable attention in scientific and industrial fields in the past two decades. A DSSCs is a photoelectrochemical system, which is composed of a porous-structured oxide film with adsorbed dye molecules as the photosensitized anode, a platinized fluorine-doped tin oxide (FTO) glass as the counter electrode (i.e., cathode), and a liquid electrolyte that traditionally contains I^-/I_3^- redox couples as a conductor to electrically connect the two electrodes.[13−18] For the counter electrode (CE), Pt plating is the key technique because Pt exhibits high electrocatalytic activity for triiodide reduction. However, because of its scarcity and costliness, finding inexpensive substitutes for Pt in the DSSCs system is crucial. At present, graphite, carbon black, carbon nanotubes, and conducting polymers have been tried as counter electrodes while their performances need to be further improved.[19−24] On the other hand, inorganic compounds were reported to be promising alternative CE materials because of their high electrocatalytic activities in reducing triiodide.[25−27]

Herein, we report our efforts on the preparation of new inorganic CE materials by choosing $CuInS_2$ as a candidate. With the help of surfactant poly(vinylpyrrolidone) (PVP, M = 40 000), $CuInS_2$ 3D microspheres could be synthesized by a one-pot solvothermal procedure. These microspheres have spongelike morphology. The reaction parameters have been optimized and the photovoltaic property has been investigated. Although there were a few papers about $CuInS_2$ nanomaterials

Received: November 13, 2013
Accepted: January 30, 2014
Published: January 30, 2014

   dx.doi.org/10.1021/am405100g | ACS Appl. Mater. Interfaces 2014, 6, 2604−2610

as CE,[28−30] with the help of reduced graphene oxide (rGO) in this DSSCs system, its power conversion efficiency has approached Pt as CE under the same conditions.

EXPERIMENTAL SECTION

Synthesis of $CuInS_2$ Microspheres. $CuInS_2$ microspheres were synthesized through a solvothermal method using CuCl, $InCl_3$ and thiourea as Cu, In and S sources, respectively, in the presence of 0.4 g of surfactant PVP and 50% n-octanol aqueous solution as solvent. The reaction was carried out at 180 °C for 24 h. The precipitate was separated by centrifugation, then washed with water and absolute ethanol to remove impurities, and the $CuInS_2$ microspheres was obtained.

Characterization. The phase of the samples was characterized by X-ray diffraction (XRD) under a Rigaku D/Max-2500 X-ray diffractometer employing Cu Kα radiation, λ = 1.54056 Å. The morphology and size of the samples were characterized by using a field emission scanning electron microscope (JEOL JSM-6700) and transmission electron microscopy (TEM, JEOL-2010, operating voltage of 200 kV), high-resolution TEM (HRTEM, JEOL-2010), AFM (Multimode8, Bruker). The Fourier transform infrared (FT-IR) spectrum was recorded with a GX spectrophotometer (Perkin -Elmer) with the KBr wafer technique.

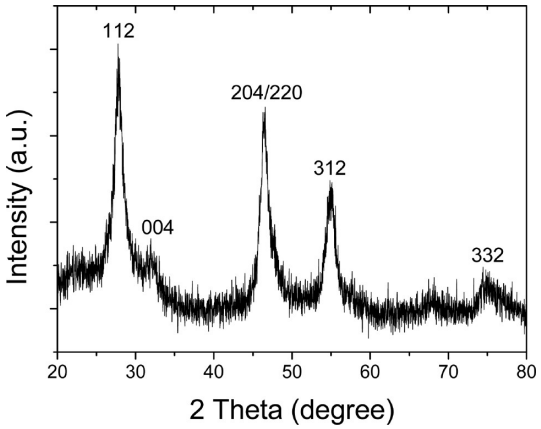

Figure 1. XRD pattern of the synthetic sample (0.4 g of PVP, 180 °C, 24 h).

Photovoltaic Performance Tests. Approximately 0.05 g of $CuInS_2$ powder was mixed with 0.5 mL of 2.5% PEG20000 solution and stirred until a fluid mixture formed. A film was then made using the doctor-blade method on FTO conductive glass (LOF, TEC-15, 15Wper square). The film was heated at 450 °C for 1 h under the protection of argon to obtain the $CuInS_2$ counter electrode. A commercial TiO_2 sol (Solaronix, Ti-Nanoxide T/SP) was used to prepare the TiO_2 film on FTO also through the doctor-blade method, and the film was soaked in an N-719 dye solution (in ethanol) for 24 h to obtain dye-sensitized TiO_2 electrodes. DSSCs were assembled by injecting the electrolyte into the aperture between the dye-sensitized TiO_2 electrode and the counter electrode. The liquid electrolyte composed of 0.05 M I_2, 0.1 M LiI, 0.6 M 1,2-dimethyl-3-propylimidazolium iodide (DMPII), and 0.5 M 4-tert-butyl pyridine with acetonitrile as the solvent. Surlyn 1702 was used as the spacer between the two electrodes. The two electrodes were clipped together and solid paraffin was used as the sealant to prevent the electrolyte solution from leaking. The effective cell area was 0.25 cm^2. Photocurrent−voltage curves were measured with a Zahner IM6ex electrochemical workstation with a Trusttech CHF-XM-500W source under simulated sun illumination (Global AM 1.5, 100 mW cm^{-2}).

RESULTS AND DISCUSSIONS

Powder X-ray diffraction (XRD) was used to characterize the crystal structure of the obtained products. As shown in Figure 1, it can be seen that the XRD pattern is in conformity with monoclinic $CuInS_2$ (a = b = 5.523 Å, c = 11.141 Å, JCPDS: 27-0159). The observed peaks could be assigned to diffractions

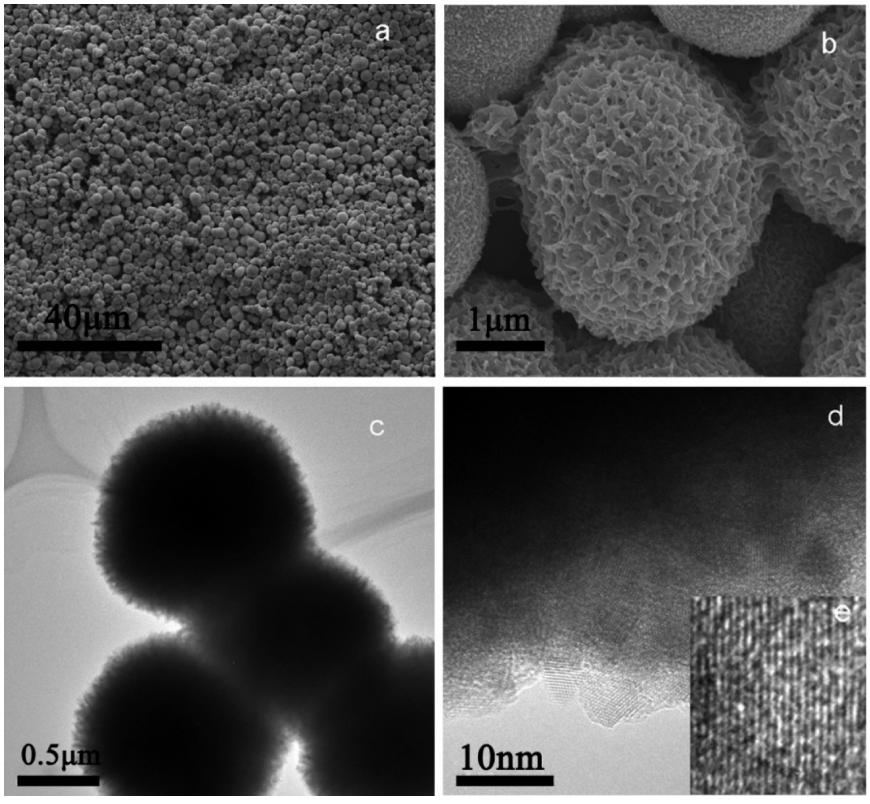

Figure 2. (a, b) SEM images of the $CuInS_2$ microspheres (0.4 g of PVP, 180 °C, 24 h): (a) low magnification, (b) high magnification. (c, d) TEM images of the $CuInS_2$ microspheres: (c) low magnification, (d) high magnification. (e) HRTEM images of the $CuInS_2$ microspheres.

dx.doi.org/10.1021/am405100g | ACS Appl. Mater. Interfaces 2014, 6, 2604−2610

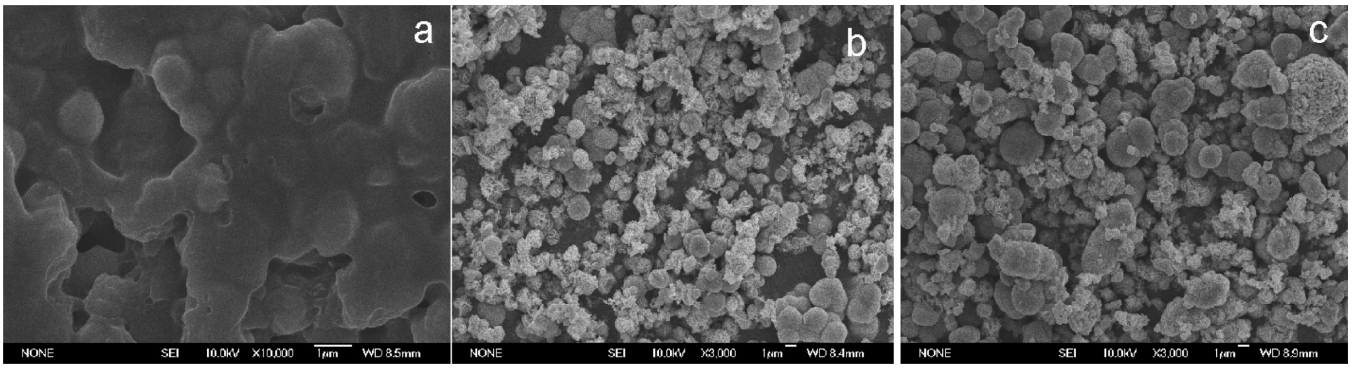

Figure 3. SEM images of the $CuInS_2$ samples prepared using different reaction times (0.4 g of PVP, 180 °C): (a) 1.5, (b) 3, and (c) 6 h.

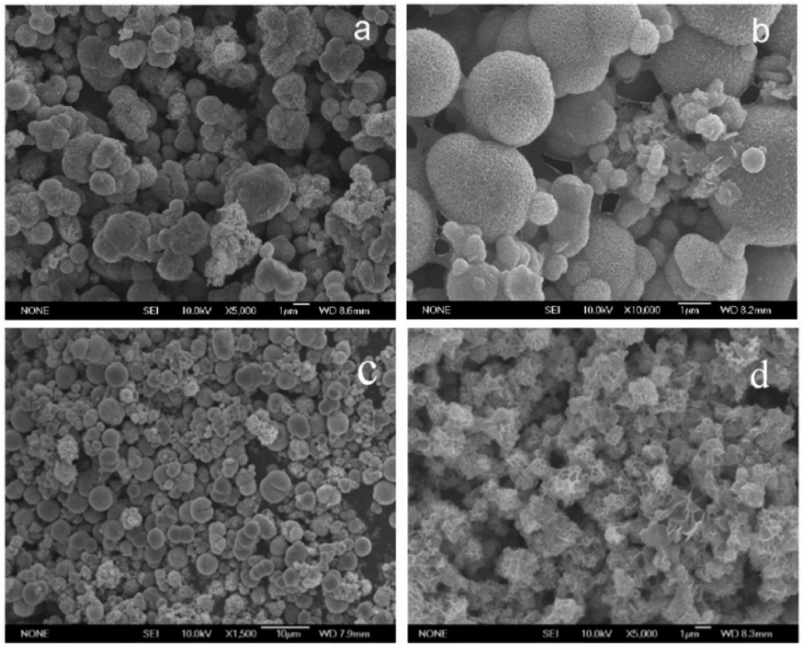

Figure 4. SEM images of the $CuInS_2$ samples prepared using different reaction conditions: (a) free PVP, (b) synthetic temperature at 150 °C, (c) H_2O as solvent, (d) n-octanol as solvent.

from the (112), (004), (204/220), (312), and (332) faces and there is no characteristic peak for other impurities such as Cu_2S and In_2S_3. This indicates that pure crystalline $CuInS_2$ was formed via the solvothermal process. Interestingly, from Figure 1 and Figure S1 in the Supporting Information, it can also be found that the relative diffraction intensities of (204/220) and (312) faces to (112) face are around 3 and 4 times higher than that of the standard values (listed in Table S1 in the Supporting Information), implying that $CuInS_2$ crystals in this sample has special growth orientations.

The morphology of the $CuInS_2$ sample was examined by scanning electron microscopy (SEM). Figure 2 shows some typical SEM images at different magnifications. As revealed in Figure 2a, 3D microspheres ranging from 0.8 to 3.7 μm in diameters could be seen obviously. The spongelike surface morphology of the microspheres could be clearly observed in Figure 2b. On the basis of the calculation applying Scherrer's equation on the XRD result (Figure 1), these microspheres are composed of small nanoparticles with an average diameter of 7.1 nm, revealing that in fact the 3D microspheres are assembled from nanoparticles. Figure 2c shows a typical transmission electron microscopy image of the $CuInS_2$ 3D superstructures. The edge portion of the 3D superstructure is lighter than that of the center, high-magnified TEM image (Figure 2d) revealed that the 3D superstructure consisted of small nanosheets, and the sheets comprised nanoparticles with diameters of 7−8 nm, consistented with XRD analysis. The high-resolution TEM image of a single nanoparticles in the microspheres shows the crystalline structure (Figure 2e). Lattice fringes with the lattice spacing of 0.19 nm, corresponding to the {220} planes of $CuInS_2$, were detected, which verified that the $CuInS_2$ crystals in this sample grew along special orientations.

To investigate the formation process of the $CuInS_2$ microspheres, we conducted time-dependent experiments with different synthetic times from 1.5 to 24 h (Figures 3 and 2), whereas the amount of surfactant PVP and reaction temperature were fixed. When very short reaction time was used (1.5 h), products of irregular morphology were obtained (Figure 3a). By gradually increasing the reaction time from 3 to 24 h, a transition procedure from mainly irregular sphere-like products to nanoparticles-assembled microspheres could be seen (Figures 3b, c and 2). A few well-structured 3D microspheres

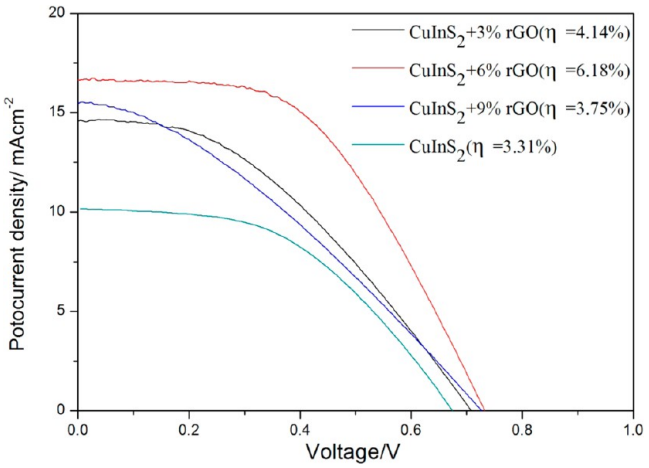

Figure 5. Photovoltage−current characteristic curves of dye-sensitized solar cells: $CuInS_2$ microspheres as counter electrodes.

were formed at 3 h (Figure 3b). As the reaction time was increased to 6 h, more and more 3D microspheres were produced (Figure 3c). By further increasing the reaction time to 24 h, nearly monodispersed microspheres could be synthesized (Figure 2). This investigation revealed that the synthetic time is a key parameter in the formation of the $CuInS_2$ 3D nanostructures.

Further experiments show that PVP, synthetic temperature, and solvent exert control over the formation of the spherical geometry and sponge-like surface morphology (Figure 4). As shown in Figure 4a, irregular microspheres with solid surface morphology were formed in the absence of surfactant PVP. The synthetic temperature has also been varied. Using low temperature (150 °C), spongelike surface morphology could be observed while the microspheres were irregular (Figure 4b). However, well-formed microspheres could be prepared at high temperatures (Figure 2 for 180 °C, see Figure S2 in the Supporting Information for 210 °C). Solvent is another key parameter for the synthesis. As shown in panels c and d in Figure 5, instead of spongelike microspheres obtained in the 1:1 mixture of H_2O and n-octanol, microspheres with solid and flowerlike surface morphologies were formed in single-component solvents of H_2O and n-octanol, respectively. This result suggested that there is a transition of surface morphology with the increasing of n-octanol. We also proved that n-octanol rather than other alcohols is crucial in this synthesis. For example, if ethanol was used in the mixed solvent, only irregular

Table 1. Photovoltaic and Electrochemical Performance Parameters for Different CEs

CE	V_{oc} (V)	J_{sc} (mA cm^{-2})	FF	η (%)	R_s (Ω cm^2)	R_1 (Ω cm^2)	R_2 (Ω cm^2)	CPE_1	CPE_2
$CuInS_2$	0.682	10.16	0.478	3.31	91.53	9.298	2.107	0.749	0.633
+3%rGO	0.71	14.59	0.40	4.14	26.18	5.958	1.114	0.734	0.764
+6%rGO	0.735	16.63	0.51	6.18	12.02	2.288	0.649	0.757	0.662
+9%rGO	0.725	15.46	0.33	3.75	41.34	5.898	1.122	0.808	0.76

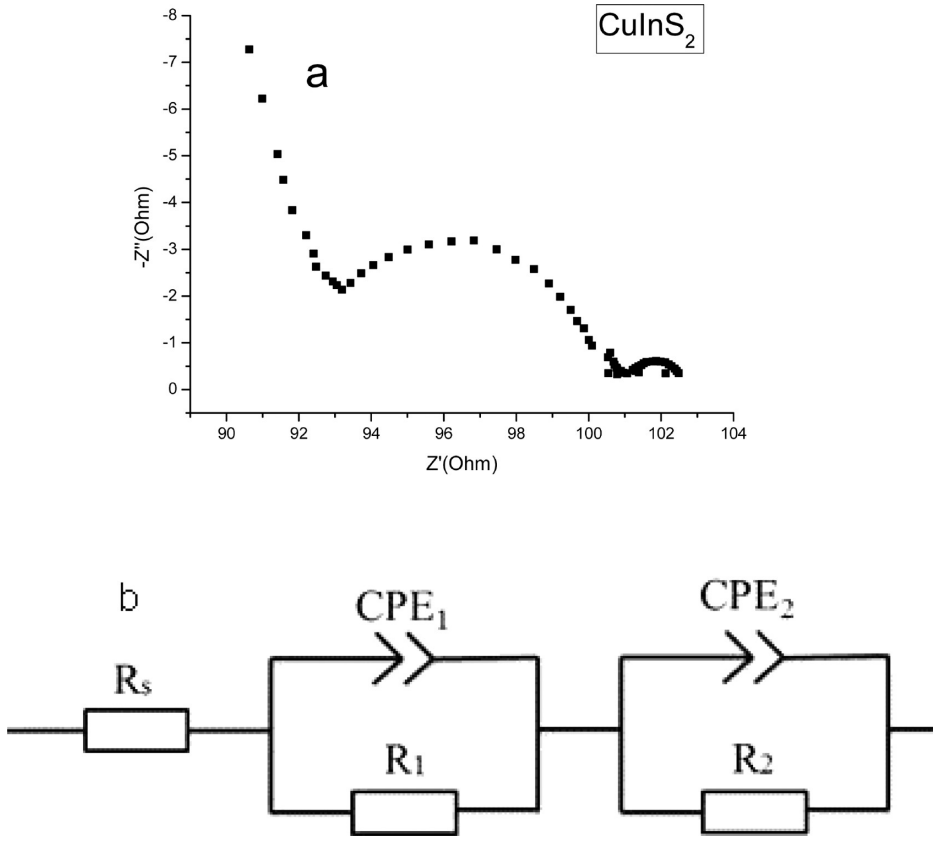

Figure 6. (a) Nyquist plots of the dummy cell fabricated with $CuInS_2$ electrodes. (b) Equivalent circuit of the symmetric device.

dx.doi.org/10.1021/am405100g | ACS Appl. Mater. Interfaces 2014, 6, 2604−2610

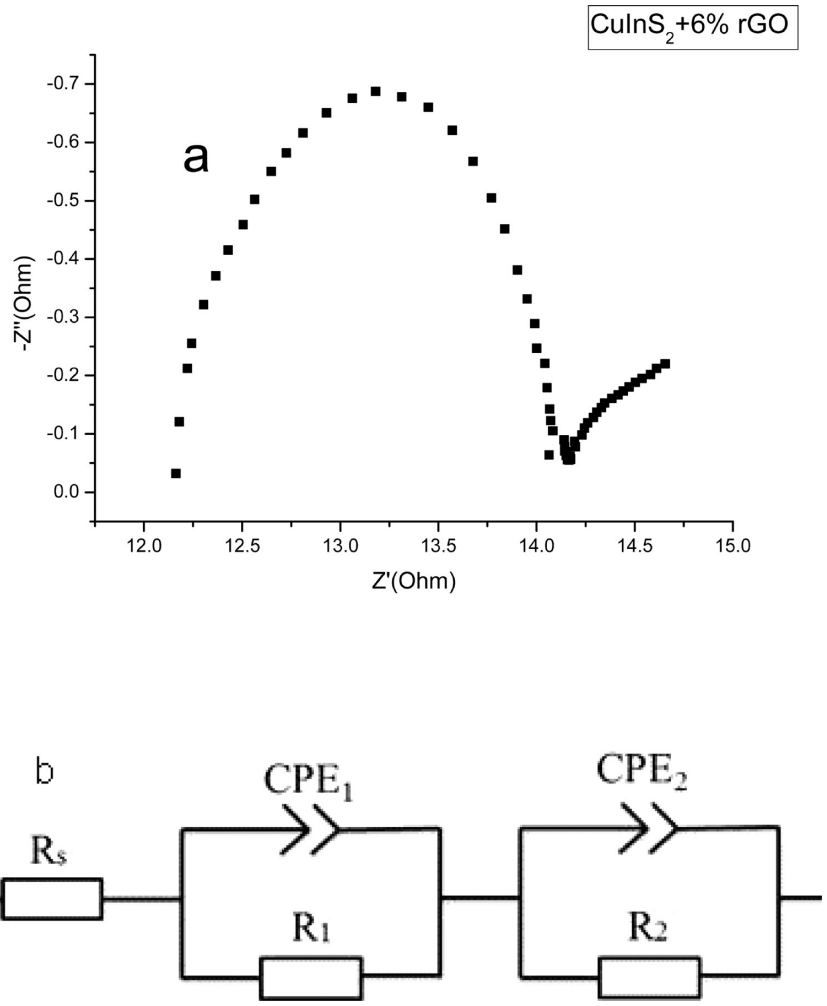

Figure 7. (a) Nyquist plots of the dummy cell fabricated with $CuInS_2$/6% rGO electrodes. (b) Equivalent circuit of the symmetric device.

microspheres were formed (see Figure S3 in the Supporting Information).

To demonstrate the potential application of the as-obtained $CuInS_2$ microspheres in dye-sensitized solar cells, we investigated the photovoltaic property. When $CuInS_2$/FTO film was used as counter electrodes (its SEM image shown in Figure S4 in the Supporting Information after calcined at 450 °C), the photovoltaic characteristics were V_{oc} = 0.682 V, J_{sc} = 10.16 mA cm^{-2}, FF = 0.478, and η = 3.31% (Figure 5). To further enhance the power conversion efficiency, we tried to add a few reduced graphene oxide (AFM image of rGO shown in Figure S5 in the Supporting Information) with as-obtained $CuInS_2$ microspheres, because it is well-known that graphene has some specific properties such as high Fermi velocity, linear energy dispersion relation, extremely high electrical mobility of both electrons and holes.[31−37] As shown in Figure 5, with the addition of rGO of 3, 6, and 9%, respectively, the CE performances have been improved substantially (for 3% rGO, V_{oc} = 0.71 V, J_{sc} = 14.59 mA cm^{-2}, FF = 0.40, and η = 4.14%; for 6% rGO, V_{oc} = 0.735 V, J_{sc} = 16.63 mA cm^{-2}, FF = 0.51, and η = 6.18%; for 9% rGO, V_{oc} = 0.725 V, J_{sc} = 15.46 mA cm^{-2}, FF = 0.33, and η = 3.75%). Especially, we found that when 6% rGO was added, a best performance of η = 6.18% could be obtained, which is slightly inferior to the Pt-based CE (η = 6.515%, see Figure S6 in the Supporting Information), but exhibited good electrocatalytic activity.

Here, $CuInS_2$ with added reduced graphene oxide as counter electrodes may attribute to the enhanced triiodide reduction or better contact between the electrolyte and the $CuInS_2$ catalyst as CoS,[38−40] which will improve the $CuInS_2$ catalytic property because of the added carbon materials.[41] Their electrochemical impendence spectroscopy (EIS) were determined. The results reveal that the addition of rGO to $CuInS_2$ improves the conductivity of the electrode (Table 1), that is, the R_s of $CuInS_2$-rGO is smaller than the Rs of $CuInS_2$, which leads to improved catalytic property of $CuInS_2$-rGO as electrode (Figures 6 and 7 and Figures S7 and S8 in the Supporting Information). The research has revealed that rGO plays the role of a binder and improves the bonding of some particles that replace Pt as counter electrodes to the FTO glass substrate. Therefore, the photoexcited electrons migrating from the TiO_2 photoanode to the surface of CE can be shuttled freely in the conducting network of graphene because the minimum of the conduction band of $CuInS_2$ is higher than the Fermi level of graphene.[42] In particular, graphene has a high surface area (theoretical value 2600 m^2/g),[43] which leads to easily capturing of electrons from redox couples (I^-/I_3^-) in the electrolyte, and thus the redox couples are easily reduced. This process can facilitate electron transmission across the CE/substrate interface. However, adding graphene leads to light absorption, and the visible light absorption is enhanced as the graphene content is increased,[44] which brings on impaired light harvesting efficiency due to

decreasing light reflected from CE to photoanode, so suitable graphene content will ensure high energy conversion efficiency. Further studies will be necessary to enhance the energy conversion efficiencies of the 3D $CuInS_2$ microspheres grown on graphene substrate.

CONCLUSION

In summary, spongelike $CuInS_2$ 3D microspheres have been synthesized through a one-step solvothermal route successfully. During the synthetic procedure the decomposition of thiourea provided S source and surfactants PVP was used to control the formation of 3D microspheres. These $CuInS_2$ 3D microspheres showed potential applications for DSSCs, which could be used as an efficient alternative for Pt. With the help of reduced graphene oxides, the energy conversion efficiency could be improved to be comparable with Pt-based counter electrode. Our method is robust, low-cost, simple, and efficient. It is also expected that this new material may find other applications such as optoelectrical devices and photocatalysis. Further studies will be necessary to enhance the energy conversion efficiencies of the 3D $CuInS_2$ microspheres grown on graphene substrate.

ASSOCIATED CONTENT

Supporting Information

Comparison of standard and experimental XRD data, SEM images, AFM image, Nyquist plots of the dummy cell fabricated with two identical $CuInS_2$/3% rGO, $CuInS_2$/9% rGO electrodes, as well as their equivalent circuit of the symmetric device. This material is available free of charge via the Internet at http://pubs.acs.org/.

AUTHOR INFORMATION

Corresponding Authors

*E-mail: liguang1971@ahu.edu.cn or liguang64@163.com.
*E-mail: xschen@mail.sitp.ac.cn.

Notes

The authors declare no competing financial interest.

ACKNOWLEDGMENTS

This work was financially supported by the State Key Program for Basic Research of China (2013CB632705), National Natural Science Foundation of China (61290301 and 11174002), and "211 Project" of Anhui University. The authors thank Prof. Y. S. Chen at Nankai University for providing graphene for this research.

REFERENCES

(1) Birkmire, R.W.; Eser, E. *Annu. Rev. Mater. Sci.* **1997**, *27*, 625−628.
(2) Kuo, K. T.; Liu, D. M.; Chen, S. Y.; Lin, C. C. *J. Mater. Chem.* **2009**, *19*, 6780−6788.
(3) Guo, Q.; Ford, G. M.; Hillhouse, H. W.; Agrawal, R. *Nano Lett.* **2009**, *9*, 3060−3065.
(4) Li, L.; Coates, N.; Moses, D. *J. Am. Chem. Soc.* **2010**, *132*, 22−23.
(5) Weil, B. D.; Connor, S. T.; Cui, Y. *J. Am. Chem. Soc.* **2010**, *132*, 6642−6643.
(6) Li, T. L.; Teng, H. S. *J. Mater. Chem.* **2010**, *20*, 3656−3664.
(7) Shi, L.; Pei, C. J.; Li, Q. *Nanoscale* **2010**, *2*, 2126−2130.
(8) Wu, J. J.; Jiang, W. T.; Liao, W. P. *Chem. Commun.* **2010**, 5885−5887.
(9) Choi, S. H.; Kim, E. G.; Hyeon, T. *J. Am. Chem. Soc.* **2006**, *128*, 2520−2521.
(10) Koo, B.; Patel, R. N.; Korgel, B. A. *Chem. Mater.* **2009**, *21*, 1962−1966.
(11) Connor, S. T.; Hsu, C. M.; Weil, B. D.; Aloni, S.; Cui, Y. *J. Am. Chem. Soc* **2009**, *131*, 4962−4966.
(12) Zheng, L.; Xu, Y.; Song, Y.; Wu, C. Z.; Zhang, M.; Xie, Y. *Inorg. Chem.* **2009**, *48*, 4003−4009.
(13) Gratzel, M. *Nature* **2001**, *414*, 338−344.
(14) Bisquert, J.; Cahen, D.; Hodes, G.; Ruhle, S.; Zaban, A. *J. Phys. Chem. B* **2004**, *108*, 8106−8118.
(15) Kroon, J. M.; Bakker, N. J.; Smit, H. J. P.; Liska, P.; Thampi, K. R.; Wang, P.; Zakeeruddin, S. M.; Gratzel, M.; Hinsch, A.; Hore, S.; Wurfel, U.; Sastrawan, R.; Durrant, J. R.; Palomares, E.; Pettersson, H.; Gruszecki, T.; Walter, J.; Skupien, K.; Tulloch, G. E. *Prog. Photovolt.* **2007**, *15*, 1−18.
(16) Longo, C.; De Paoli, M. A. *J. Braz. Chem. Soc.* **2003**, *14*, 889−901.
(17) Martinson, A. B. F.; Hamann, T. W.; Pellin, M. J.; Hupp, J. T. *Chem.—Eur. J.* **2008**, *14*, 4458−4467.
(18) Gratzel, M. *Prog. Photovolt.* **2000**, *8*, 171−185.
(19) Murakami, T.; Gratzel, M. *Inorg. Chim. Acta* **2008**, *361*, 572−580.
(20) Trancik, J. E.; Barton, S. C.; Hone, J. *Nano Lett.* **2008**, *8*, 982−987.
(21) Xia, J.; Masaki, N.; Jiang, K.; Yanagida, S. *J. Mater. Chem.* **2007**, *17*, 2845−2850.
(22) Seo, S. H.; Kim, S. Y.; Koo, B. K.; Cha, S. I.; Lee, D. Y. *Langmuir* **2010**, *26*, 10341−10346.
(23) Joshi, P.; Zhang, L. F.; Chen, Q. L.; Galipeau, D.; Fong, H.; Qiao, Q. Q. *ACS Appl. Mater. Interfaces* **2010**, *2*, 3572−3577.
(24) Hou, S. C.; Cai, X.; Fu, Y. P.; Lv, Z. B.; Wang, D.; Wu, H. W.; Zhang, C.; Chu, Z. Z.; Zou, D. C. *J. Mater. Chem.* **2011**, *21*, 13776−13779.
(25) Wang, M. K.; Anghel, A. M.; Marsan, B.; Ha, N. C.; Pootrakulchote, N.; Zakeeruddin, S. M.; Grätzel, M. *J. Am. Chem. Soc.* **2009**, *131*, 15976−15977.
(26) Jiang, Q. W.; Li, G. R.; Gao, X. P. *Chem. Commun.* **2009**, 6720−6722.
(27) Li, G. R.; Wang, F.; Jiang, Q. W.; Gao, X. P.; Shen, P. W. *Angew. Chem., Int. Ed.* **2010**, *49*, 3653−3656.
(28) Liu, Y. F.; Xie, Y.; Cui, H. L.; Zhao, W.; Yang, C. Y.; Wang, Y. M.; Huang, F. Q.; Dai, N. *Phys. Chem. Chem. Phys.* **2013**, *15*, 4496−4499.
(29) Yao, R. Y.; Zhou, Z. J.; Hou, Z. L.; Wang, X.; Zhou, W. H.; Wu, S. X. *ACS Appl. Mater. Interfaces* **2013**, *5*, 3143−3148.
(30) Zhang, X. L.; Huang, X. M.; Yang, Y. Y.; Wang, S.; Gong, Y.; Luo, Y. H.; Li, D. M.; Meng, Q. B. *ACS Appl. Mater. Interfaces* **2013**, *5*, 5954−5960.
(31) Novoselov, K. S.; Geim, A. K.; Morozov, S. V.; Jiang, D.; Zhang, Y.; Dubonos, S. V.; Grigorieva, I. V.; Firsov, A. A. *Science* **2004**, *306*, 666−669.
(32) Novoselov, K. S.; Geim, A. K.; Morozov, S. V.; Jiang, D.; Katsnelson, M. I.; Grigorieva, I. V.; Dubonos, S. V.; Firsov, A. A. *Nature* **2005**, *438*, 197−200.
(33) Zhang, Y.; Tan, J. W.; Stormer, H. L.; Kim, P. *Nature* **2005**, *438*, 201−204.
(34) Avouris, P.; Chen, Z.; Perebeinos, V. *Nat. Nanotechnol.* **2007**, *2*, 605−615.
(35) Geim, A. K.; Novoselov, K. S. *Nat. Mater.* **2007**, *6*, 183−191.
(36) Rao, C. N. R.; Biswas, K.; Subrahmanyam, K. S.; Govindaraj, A. *J. Mater. Chem.* **2009**, *19*, 2457−2469.
(37) Rao, C. N. R.; Sood, A. K.; Subrahmanyam, K. S.; Govindaraj, A. *Angew. Chem., Int. Ed.* **2009**, *48*, 7752−7777.
(38) Toivola, M.; Peltokorpi, L.; Halme, J.; Lund, P. *Sol. Energy Mater. Sol. Cells* **2007**, *91*, 1733−1742.
(39) Andrade, L.; Zakeeruddin, S. M.; Nazeeruddin, M. K.; Ribeiro, H. A.; Mendes, A.; Gratzel, M. *ChemPhysChem* **2009**, *10*, 1117−1124.
(40) Zaban, A.; Zhang, J.; Diamant, Y.; Melemed, O.; Bisquert, J. *J. Phys. Chem. B* **2003**, *107*, 6022−6025.
(41) Zhang, Z. Y.; Zhang, X. Y.; Xu, H. X.; Liu, Z. H.; Pang, S. P.; Zhou, X. H.; Dong, S. M.; Chen, X.; Cui, G. L. *ACS Appl. Mater. Interfaces* **2012**, *4*, 6242−6246.

(42) Long, R.; English, N. J.; Prezhdo, O. V. *J. Am. Chem. Soc.* **2012**, *134*, 14238−14248.
(43) Stankovich, S.; Dikin, D. A.; Dommett, G. H. B.; Kohlhaas, K. M.; Zimney, E. J.; Stach, E. A.; Piner, R. D.; Nguyen, S. B. T.; Ruoff, R. S. *Nature* **2006**, *442*, 282−286.
(44) Kim, H. N.; Yoo, H.; Moon, J. H. *Nanoscale* **2013**, *5*, 4200−4204.